

3D crustal structure of the Jammu and Kashmir Himalaya: signatures of mid-crustal ramp and Lesser Himalayan duplex

Supriyo Mitra¹, Swati Sharma^{1,2}, Sunil Kumar Wanchoo², Keith Priestley³

¹Department of Earth Sciences, Indian Institute of Science Education and Research Kolkata, Mohanpur, West Bengal, India

²School of Physics, Shri Mata Vaishno Devi University, Katra, India

³Bullard Laboratories, Department of Earth Sciences, University of Cambridge, UK

Key Points:

- Underthrust Indian crust beneath J&K, dips gently NE. Moho depth ~ 45 km (Shiwalik) to ~ 70 km (Tethyan Himalaya), undulations, southward dip
- Main Himalayan Thrust (Kishtwar) flat-ramp geometry. Flat dip $\sim 4^\circ$, mid-crustal ramp ~ 13 – 17° , Lesser Himalayan Duplex has moderate seismicity
- Kashmir Valley thicker crust, higher V_s shallow MHT. Linked by SE dipping MHT lateral ramp, seismicity on frontal-lateral ramp intersection

Corresponding author: Supriyo Mitra, supriyomitra@iiserkol.ac.in

Abstract

We use teleseismic data from the Jammu and Kashmir Seismological NETWORK, to perform P-wave receiver function spatial and common-conversion-point (CCP) stacks, and joint inversion with Rayleigh-wave group-velocity dispersion, to construct 3D V_s model of the Jammu and Kashmir (J&K) Himalaya. 2D CCP and V_s profiles reveal increasing crustal thickness from the foreland-to-hinterland, and an under-thrust Indian crust beneath J&K. The Moho positive impedance-contrast boundary is at ~ 45 km depth beneath Sub-Himalaya and deepens to ~ 70 km beneath Higher-to-Tethyan Himalaya, with an overall gentle NE dip. The Main Himalayan Thrust (MHT) forms a low velocity layer (LVL) with negative impedance contrast, and has a flat-ramp geometry. The flat segment is beneath Sub-to-Lesser Himalaya at 6–10 km depth, and dips $\sim 4^\circ$. The mid-crustal (frontal) ramp is beneath Kishtwar Higher-Himalaya and Zaskar Ranges at 10–16 km depth, and dips ~ 13 – 17° . Significant along-arc variation in crustal structure is observed between east (Kishtwar) and west (Kashmir Valley) segments. Beneath the Kishtwar Window we image a Lesser Himalayan duplex (LHD) bound between MHT sole-thrust and MCT roof-thrust. LHD horizons dip at high angle to the bounding structures and are illuminated by moderate seismicity. Beneath the Pir-Panjal Ranges and Kashmir Valley, the underthrust crust is ~ 10 km thicker, has higher crustal V_s , and a shallower flat MHT at ~ 10 km depth. The westward shallowing of the MHT occurs through a lateral ramp beneath Kishtwar Himalaya. Aftershocks of the 2013 Kishtwar earthquake concentrate on the MHT frontal and lateral ramp intersection, and possibly marks the down-dip locked-to-creep transition.

Plain Language Summary

We model the 3D-seismic-velocity structure of the Jammu & Kashmir (J&K) Himalaya using teleseismic data from the Jammu and Kashmir Seismological NETWORK. The network extends from the Sub-Himalaya (south) to Tethyan Himalaya (north), across Himalayan thrust-systems and litho-tectonic units. We use body-wave conversion and reverberations within the crust to construct 2D profiles, and perform joint modeling with surface-wave dispersion data to compute 3D velocity model. Our results reveal under-thrust Indian crust beneath J&K Himalaya. The Moho at the base of the Indian crust is a positive impedance contrast boundary with increasing depth from foreland (~ 45 km) to hinterland (~ 70 km). The Main Himalayan Thrust (MHT), between the top of the

under-thrust Indian crust and overriding Himalayan wedge, is a low velocity layer with negative impedance contrast. The MHT has flat-ramp geometry beneath Kishtwar Himalaya, with $\sim 4^\circ$ dipping flat and $\sim 1317^\circ$ dipping mid-crustal (frontal) ramp. A Lesser Himalayan Duplex overlies the MHT beneath Kishtwar Window and is illuminated by moderate earthquakes. Along-arc the crust thickens by ~ 10 km to the west beneath Kashmir Valley and MHT shallows through a SE-dipping lateral ramp. Aftershocks of the 2013 Kishtwar earthquake concentrate on MHT frontal and lateral ramp intersection, at the down-dip locked-to-creep transition.

1 Introduction

Continent-Continent collision between the Indian and Eurasian plates have resulted in the formation of the highest mountain ranges, the Himalaya, and the largest plateau, the Tibetan Plateau. The ongoing convergence occurs at ~ 38 mm yr $^{-1}$ and is accommodated across a width of ~ 2000 km (Wang & Shen, 2020). The Himalayan Mountains form the southern boundary of this convergence zone and absorb almost half of the ongoing convergence (Stevens & Avouac, 2015). This occurs through under-thrusting of the Indian Plate beneath the Himalaya and southern Tibet along a basal detachment known as the Main Himalayan Thrust (MHT) (Priestley et al., 2019). The MHT marks the top of the down-going Indian crust and its shallow up-dip segment is frictionally locked, while the deeper segment creeps aseismically (Bilham et al., 2001). In response to the ongoing convergence and built-up of elastic strain, the locked segment of the MHT ruptures occasionally in major-to-great earthquakes (Bilham, 2019). In the past two centuries at least six major earthquakes ($M_w > 7.5$) have ruptured the MHT, either partially or completely (Fig. 1a). However, three distinctive segments in the west, center and east, have not had a major earthquake in the past ~ 500 years. From geodetic measurements, it is known that these segments have been accumulating elastic strain and are capable of driving a future major-to-great earthquake (Ader et al., 2012; Stevens & Avouac, 2015). These are referred to as "seismic gaps" (Khatti, 1987; Bilham, 2019). This study focuses on the seismic gap in the north-western Himalaya across Jammu and Kashmir (J&K).

The J&K Himalayan seismic gap lies between the rupture areas of the 1905 Kangra earthquake (M_w 7.9) and the 2005 Muzaffarabad earthquake (M_w 7.6), and straddles the meiseisomal zone of the 1555 Kashmir earthquake ($M_w \sim 8.0$) (Bilham, 2019).

This region lies immediately east of the northwest syntaxis and spans along-arc from the Kashmir Valley, in the west, to the Kishtwar Window, in the east. Across the J&K Himalayan arc (south to north) the major litho-tectonic units are the Himalayan Foreland Basin, the Sub-Himalaya, the Lesser Himalaya, the Higher Himalaya and the Tethyan Himalaya. The Himalayan Foreland Basin has Quaternary-to-Recent sedimentary formations. This is separated from the Sub-Himalaya by an anticlinorium, called the Surin Mastgarh Anticline (SMA). The Main Frontal Thrust (MFT), the southernmost splay fault from the MHT, is buried below the SMA (Thakur & Rawat, 1992). Majority, or all of the present-day active convergence across this region is accommodated by this fault underlying the SMA (Schiffman et al., 2013; O’Kane et al., 2022). The Sub-Himalaya consists of Oligocene-Pliocene Foreland Basin deposits and are further subdivided into the Shiwalik (south) and Murree (north) Formations (Gavillot et al., 2016). These formations are separated by a series of en-echelon faults, stepping from east-to-west, the Mandli-Kishanpur Thrust (MKT), the Reasi Thrust (RT), the Kotli Thrust (KT) and the Balakot-Bagh Fault (BBF). The BBF hosted the 2005 Muzzafarabad earthquake with a surface rupture of ~ 150 km (Avouac et al., 2006; Powali et al., 2020). The Reasi Thrust has been shown to accommodate long-term shortening of $5\text{--}6$ mm yr $^{-1}$, and has exhumed Precambrian limestone to the surface (Gavillot et al., 2016). North of the Sub-Himalaya is the Lesser Himalaya consisting of the Proterozoic low-grade meta-sediments. The Main Boundary Thrust (MBT) separates the Sub-Himalaya from the Lesser Himalaya. North of the Lesser Himalaya is the Higher Himalayan low-grade and high-grade crystalline rocks of late Precambrian to early Paleozoic age. The Main Central Thrust (MCT) separates the Lesser and Higher Himalayas. The MBT and MCT lie within 10–20 km of each other throughout the J&K Himalaya and runs along the southern slope of the Pir-Panjal Ranges, in the west. Across the eastern segment (referred to as the Jammu-Kishtwar Himalaya, henceforth), within the Higher Himalaya, lies the Kishtwar Window exposing Lesser Himalayan units. This is interpreted to be an anti-formal stack-duplex (Lesser Himalayan Duplex - LHD) with the MHT and MCT acting as the sole and roof thrusts, respectively. The Kishtwar Window LHD exposes structurally deeper level rocks compared to its surrounding Higher Himalaya. Immediately west of Jammu the MFT, RT and further north the MBT and MCT retreats towards the hinterland in a sharp bend, forming a reentrant structure. Further to the west is the Kashmir Valley, an intermontane basin formed atop the Higher Himalayan crystalline rocks. The Valley is bound to the south by the Pir-

Panjal Ranges and to the north by the Zaskar Ranges. The Zaskar Shear Zone (ZSZ) skirts the Valley to the south and east and carries Tethyan Himalayan strata, which are exposed in the Pir-Panjal Ranges, the Kashmir Valley and the Zaskar Ranges (Gavillot et al., 2016). The ZSZ is an equivalent of the Southern Tibetan Detachment (STD) in west-central Himalaya and continues eastward north of the Kishtwar Window. From balanced cross-section reconstruction and geochronological studies it has been interpreted that the style of deformation across the Jammu-Kishtwar Himalaya is different from the Kashmir Valley. The across-arc shortening across Jammu-Kishtwar Lesser and Higher Himalaya was accommodated by discrete under-plating and Lesser Himalayan duplexing, while frontal accretion was the dominant mechanism across the Kashmir Valley (Gavillot et al., 2016; Yu et al., 2015). Such differences are expected to necessitate lateral variation in crustal structure and flat-ramp geometry on the MHT. Absence of sub-surface images have till-date severely limited the testing of these hypothesis.

Crustal structure of the Kashmir Valley have been studied by Mir et al. (2017) using eight broadband seismograph stations. They produced a NE-SW 2D profile across the Kashmir Basin, which revealed a gently dipping Moho from ~ 40 – 60 km depth and a relatively flat MHT at ~ 12 – 16 km depth. The 3D nature of the crust beneath the Kashmir Himalaya and their limited number of broadband stations restricted any scope of ascertaining lateral variation in crustal structure or deciphering details of the Himalayan wedge and MHT. No knowledge of the crustal structure beneath the Jammu–Kishtwar Himalaya are available till date. We present new data and analysis from one of the largest broadband seismological deployments in the Jammu and Kashmir Himalaya (Sharma et al., 2020). We use P-wave receiver function analysis to present (i) 2D common conversion point (CCP) stack profiles and (ii) 3D V_s models obtained from joint inversion of receiver functions and Rayleigh wave group velocity dispersion data. Our study provides (a) 3D crust and upper mantle V_s structure of the Jammu and Kashmir Himalaya, (b) the geometry of the Moho, and the MHT, and (c) variation in structure of the Himalayan wedge beneath Jammu–Kishtwar Himalaya and Kashmir Valley. Our V_s models are presented along with the distribution of aftershocks of the 2013 Kishtwar earthquake (Paul et al., 2018) to decipher the geometry and seismogenic behavior of the MHT. The CCP profiles are combined with fault-plane geometry of moderate earthquakes ($5.0 < M_w < 5.9$) on and above the MHT (O’Kane et al., 2022) to highlight the internal structure of the

Himalayan orogenic wedge. Finally, we provide insights into the along-arc variations in models of long-term shortening across the NW Himalaya.

2 JAKSNET Data

The data for this study has been recorded by the Jammu and Kashmir Seismological NETWORK (JAKSNET), established in July 2013 through an international collaboration between Indian Institute of Science Education and Research Kolkata, Shri Mata Vaishno Devi University Katra, and the University of Cambridge UK. JAKSNET is the first deployment of a dense network of seismological stations in Jammu and Kashmir Himalaya and consist of 20 stations (Fig. 1b and Table 1). Each station is equipped with a 3-component broadband seismograph system (either a CMG-3T or a CMG-3ESPCD) and recorded continuous ground motion data at 100 Hz. Station location and time-stamping of the data is done using Global Positioning System (GPS) receivers. Further details about the network and data quality are available in Sharma et al. (2020). For this study we used teleseismic earthquakes recorded from July 2013 to June 2019, in the distance range of 30–90°, with magnitude (M_w) greater than 5.0 (Fig. 1c). A total of 1353 earthquakes, spread over a large back-azimuth range, have been used for our analysis.

3 Receiver Function Analysis

To model the crustal structure of the Jammu and Kashmir Himalaya we use teleseismic P-wave receiver function (P-RF) analysis and joint inversion of P-RFs with Rayleigh wave dispersion data. P-RF comprises P-to-SV conversion and reverberations beneath the seismograph station, generated by the interaction between the teleseismic P-wave and the underlying structure (Langston, 1977; Owens et al., 1984; Priestley et al., 1988). The 3-component broadband waveform data is recorded as vertical (Z), and two horizontal components, north-south (N) and east-west (E). The horizontal components are rotated into the radial (R) and tangential (T) components, using the earthquake–station back-azimuth. This isolates the P-SV energy into the vertical–radial plane for a 1D isotropic structure. The classical P-RF computation technique requires removal of the source and common-path propagation effects, by frequency-domain deconvolution of the Z component from the R and T components (C. Ammon et al., 1990; C. J. Ammon, 1991). These generate radial and tangential P-RFs. However, for noisy data with spectral holes in the Z component, the computed radial P-RF can be unstable (Huang et al., 2015). This is

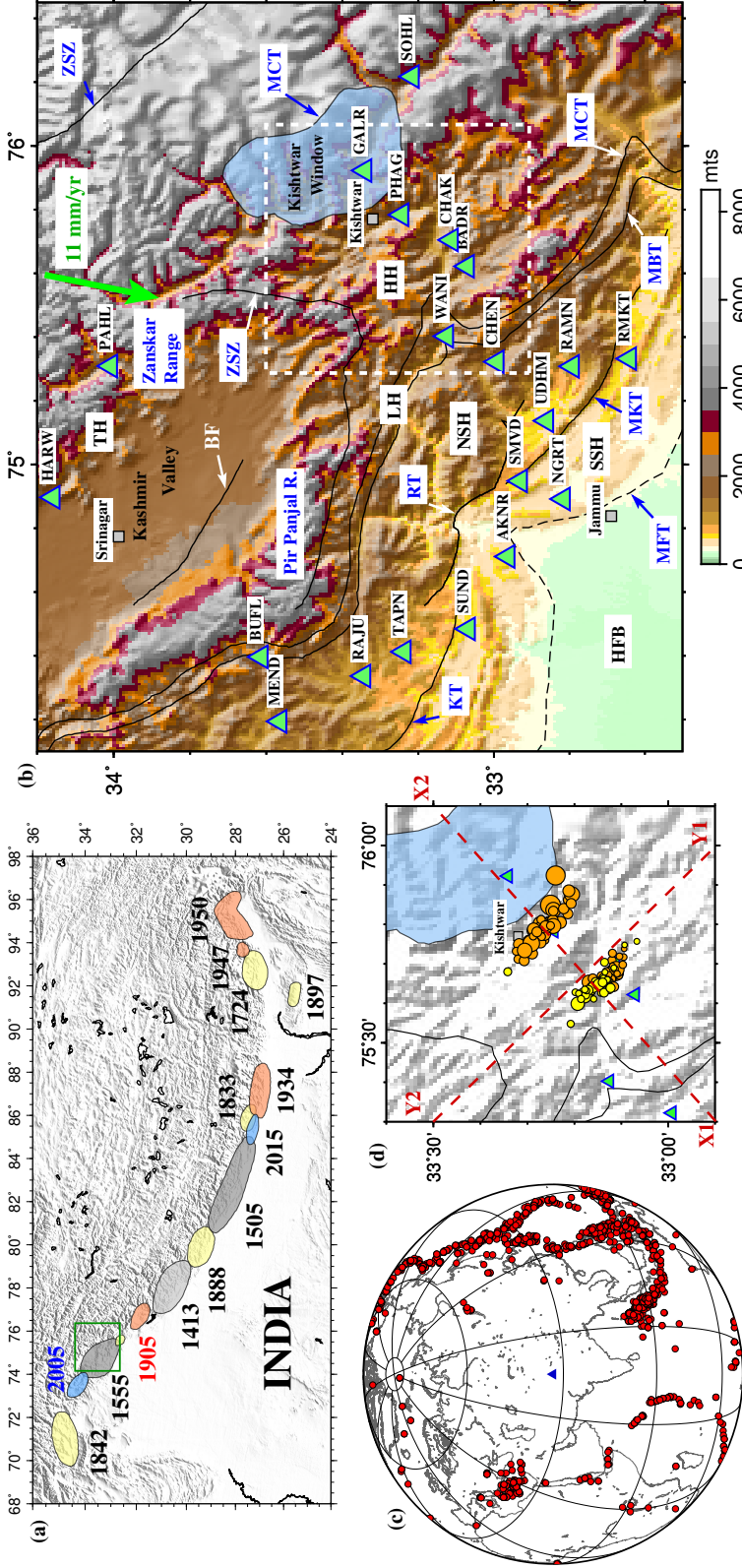


Figure 1. (a) Map of the Himalaya with past major earthquakes plotted as colored ellipses and their year of occurrence written beside the ellipse. The ellipses are color coded as: blue - this century, orange - 19th century, yellow - 18th century and grey - 17th century and before. The region of our study in the Jammu and Kashmir Himalaya is marked by a green box. (b) Topographic map of the Jammu and Kashmir Himalaya, with plot of the seismograph stations (green triangles). The arc-normal convergence rate of 11 mm yr⁻¹ (Schiffman et al., 2013) is shown as a green arrow. The tectonic units are labeled as: HFB - Himalayan Foreland Basin, SSH - Southern Sub-Himalaya, NSH - Northern Sub-Himalaya, LH - Lesser Himalaya, HH - Higher Himalaya, TH - Tethyan Himalaya, MFT - Main Frontal Thrust, MKT - Main Boundary Thrust, MBT - Main Central Thrust, BF - Balapora Fault, ZSZ - Zaskar Shear Zone. (c) Plot of earthquakes (red circles) used for receiver function analysis. Average location of stations plotted as a blue triangle. (d) Zoomed in map of the Jammu-Kishtwar Higher Himalaya (white dashed box in (b)) with plot of earthquakes taken from Paul et al. (2018). Size of circles scaled by earthquake magnitude and color coded for depth. Yellow is <10 km and orange is 10–20 km.

No.	Station Code	Lat. (°N)	Long. (°E)	Elev. (m)	Total RFs	Best RFs	Moho (km)	J&K Himalayan Region
1	AKNR	32.9631	74.7114	550	219	83	42±2	S Sub-Himalaya
2	NGRT	32.8167	74.8920	392	255	72	42±2	S Sub-Himalaya
3	SMVD	32.9302	74.9486	643	710	227	58±2	S Sub-Himalaya
4	RMKT	32.6412	75.3323	682	682	245	42±2	S Sub-Himalaya
5	SUND	33.0678	74.4844	590	530	191	60±2	S Sub-Himalaya
6	UDHM	32.8607	75.1374	704	573	157	42±2	N Sub-Himalaya
7	RAMN	32.7926	75.3080	860	625	236	52±2	N Sub-Himalaya
8	CHEN	32.9921	75.3224	1465	490	229	55±2	N Sub-Himalaya
9	TAPN	33.2375	74.4124	762	390	167	60±2	N Sub-Himalaya
10	RAJU	33.3438	74.3363	918	388	62	54±2	N Sub-Himalaya
11	MEND	33.5647	74.1941	1452	532	155	58±2	N Sub-Himalaya
12	WANI	33.1254	75.4028	1221	397	175	53±2	Lesser Himalaya
13	BUFL	33.6139	74.3964	1867	642	133	56±2	Lesser Himalaya
14	BADR	33.0707	75.6220	1521	849	457	52±2	Higher Himalaya
15	CHAK	33.1129	75.7047	1500	169	31	58±2	Higher Himalaya
16	PHAG	33.2439	75.7837	1141	358	150	53±2	Higher Himalaya
17	GALR	33.3412	75.9225	1788	133	86	53±2	Kishtwar Window
18	SOHL	33.2160	76.2176	2047	182	78	66±2	Higher Himalaya
19	HARW	34.1583	74.8971	1650	544	126	58±2	Tethyan Himalaya (KV)
20	PAHL	34.0084	75.3089	2220	370	182	66±2	Tethyan Himalaya (ZR)

Table 1. List of stations, location, total number of P-RFs, best P-RFs (used in this analysis), average crustal thickness/Moho depth (Sharma, 2020) and Himalayan region where the station is located.

overcome by using an iterative time-domain deconvolution technique (Ligorria & Ammon, 1999), where a spike train is constructed by cross-correlating the R with Z component. This spike-train is convolved with the observed Z component to produce a synthetic R component. The difference between the synthetic and observed R components is computed in the least-squares sense and the misfit value is used to update the spike-train. The above process is repeated (iterated) using the updated spike-train till the misfit becomes smaller than a cut-off value (set to 0.001) or 200 iterations (set as maximum) are completed. The best-fitting spike train, obtained in this iterative manner, is the estimated P-RF. A Gaussian filter is applied to the waveform to eliminate high-frequency noise and stabilize the time-domain deconvolution. We choose a Gaussian filter of width 2.5 (maximum frequency ~ 1.2 Hz) to low-pass filter the waveforms. The quality of the estimated P-RFs is ascertained by the percentage fit between the calculated and observed radial waveforms. An 80% cut-off fit value has been used for the estimated P-RFs, in this study. Data from all JAKSNET stations are processed using the above procedure, and a list of total P-RFs and best P-RFs (i.e. above 80% fit) is given in Table 1.

To study the crustal structure, its lateral variation and the disposition of the major impedance contrast interfaces, the P-RFs are used to construct (a) 2D profiles using common conversion point (CCP) stacking method, across and along the Jammu and Kashmir Himalaya; and (b) 3D maps of V_s structure through joint modeling of P-RFs with published Rayleigh-wave group velocity dispersion data. The methodology involved in these 2D and 3D imaging techniques are briefly described below.

3.1 2D Common Conversion Point (CCP) Stack

Depth migrated common conversion point stacking of phase conversions and reverberations, of the observed P-RFs, enhances coherent signal from impedance contrast boundaries (Dueker & Sheehan, 1997). This is done along 2D profiles using the technique of Zhu (2000). The P-RFs at each station are projected backward along the ray using ray-theory, through a modified IASP91 velocity model (Kennett & Engdahl, 1991). The IASP91 velocity model is modified by changing (increasing) the crustal thickness taken from joint inverted V_s models (Sharma, 2020) (Table 1). The arrival times of the P-RF converted (Ps) and reverberated (PpP_{ms}, PpS_{ms} + PsP_{ms}) phases are depth migrated below the surface, therefore taking into account the elevation of the stations. Based on the inclination of the rays, the P-RF amplitudes are corrected for incidence-angle effect and binned

in narrow horizontal and vertical bins. For our analysis we choose bin size of 1 km in both directions. The P-RF amplitudes within each bin (representing common conversion points in space) are stacked (averaged) and normalized by the number of piercing rays within the bin. This allows the CCP stacked amplitudes to be plotted as a fraction of the direct P-wave amplitude (set to unity). The CCP stacking technique enhances coherent signal and cancels incoherent noise. Depth migration, binning and stacking are performed for conversion and reverberations, which enhances the wave-field and makes it coherent in all three phases. This significantly improves imaging of the shallow sub-surface structures.

3.2 3D Shear-wave Velocity Structure

The region between longitudes 74° and 76.4° , and latitudes 32.4° and 34.4° is divided into square grids of 0.1° sides (Fig. 2a). Piercing points of P-RFs have been calculated at average mid-crustal depth of 30 km using the Taup toolkit (Crotwell et al., 1999) (Fig. 2a). P-RFs with piercing points lying within each grid are stacked together to form an average P-RF (also referred to as the P-RF stack) representative of the grid (Fig. 2b,c,d). Rayleigh wave group velocity dispersion data for periods 5–70 s, corresponding to the center point of each grid, has been taken from Gilligan and Priestley (2018) (Fig. 2e). These two complementary datasets have been jointly inverted to model the shear-wave velocity (V_s) structure of the crust and uppermost mantle (Fig. 2f). P-RFs constrain the impedance contrast boundaries beneath a receiver site and the Rayleigh wave group velocity dispersion is sensitive to the vertical-averages of the shear-wave velocity structure. The depth sensitivity of the Rayleigh wave dispersion dataset is period (frequency) dependent, with increasing periods sampling greater depth. The 1D V_s models obtained from the inversion are interpolated in x-y-z to form 3D V_s model for the Jammu and Kashmir Himalaya.

We use the linearized-least-squares inversion algorithm of Herrmann and Ammon (2004), which is an implementation of Julià et al. (2000), to perform the joint inversion of the two datasets. The starting/initial model for the inversion is constructed as a mantle half-space with V_s of 4.7 km s^{-1} , based on the modeled upper mantle V_s beneath the Indian Shield (Mitra et al., 2006) (Fig. 2f). This model is parameterized as thin layers upto 150 km underlain by a mantle half-space. The layer thicknesses are 0.5 km (4 layers), 1 km (2 layer), 2 km (48 layers) and 10 km (5 layers). The choice of total depth

of 150 km for the layered model is based on the sensitivity of the dispersion dataset. An a-priori weighting parameter (between 0 and 1) is used to control the influence of each data set in the inversion. We assigned 80% weight to the P-RF stack and 20% to the dispersion data, respectively. The choice of weights is based on previous literature (Mitra et al., 2018) and through tests of best fit between the synthetic and observed dataset. The final model matches the most significant arrivals of the P-RFs and the synthetics lie within $\pm 1\sigma$ bounds of the observed (Fig. 2e,f). Quantitatively, we achieve a minimum acceptable fit of 99% for the dispersion data and 95% for the P-RFs.

4 Results

Our results are presented in three parts as follows. First, we present three 2D profiles comprising spatially stacked P-RFs, CCP stacks and 2D V_s models along profiles (Figs. 3, 4 and 5). Second, we present 2D maps of absolute V_s , averaged over 10 km intervals between 0 and 40 km, and V_s anomaly maps, calculated as deviations from the average V_s in that depth range (Fig. 6). Third, we present maps of average crustal V_s and thickness, estimated using uppermost mantle V_s of 4.3 km s^{-1} (Fig. 7). The Moho map is compared with the Moho depths obtained from joint inversion of P-RFs (stacked in narrow bins of back-azimuth at each station) and Rayleigh wave group velocity dispersion (Sharma, 2020). The first two 2D profiles have been chosen across the Himalayan arc (SW-NE), such that a comparison can be made between the structure beneath Jammu-Kishtwar Himalaya and the Pir-Panjal Ranges, Kashmir Valley and Zaskar Ranges. The third one is sub-parallel to the strike of the arc (SSE-NNW), over the western Sub-Himalaya, starting at the edge of the Foreland Basin to south of the MBT. In all these profiles, the three most significant P-RF arrivals are the positive Ps conversion at the Moho and the mid-crustal discontinuity, and the negative Ps conversion at the MHT.

The Jammu-Kishtwar profile is oriented SW-NE, starting from the Foreland Basin sediments, immediately west of Jammu, across the southern Sub-Himalaya/Shiwalik (NGRT and SMVD), the northern Sub-Himalaya/Murree (UDHM, RAMN and CHEN), the Lesser Himalaya (WANI), the Higher Himalaya (BADR, CHAK, PHAG and SOHL) and the Kishtwar Window (GALR) (A1–A2 Fig. 2a). The Moho Ps phase is the strongest conversion at $\sim 5.5 \text{ s}$ beneath the Shiwalik; abruptly deepens to $\sim 7 \text{ s}$ beneath SMVD in the northern Sub-Himalaya and reverts back to $\sim 5.5 \text{ s}$ immediately to its north (UDHM) (Fig. 3c). This appears like a discontinuous Moho segment, which will be discussed later.

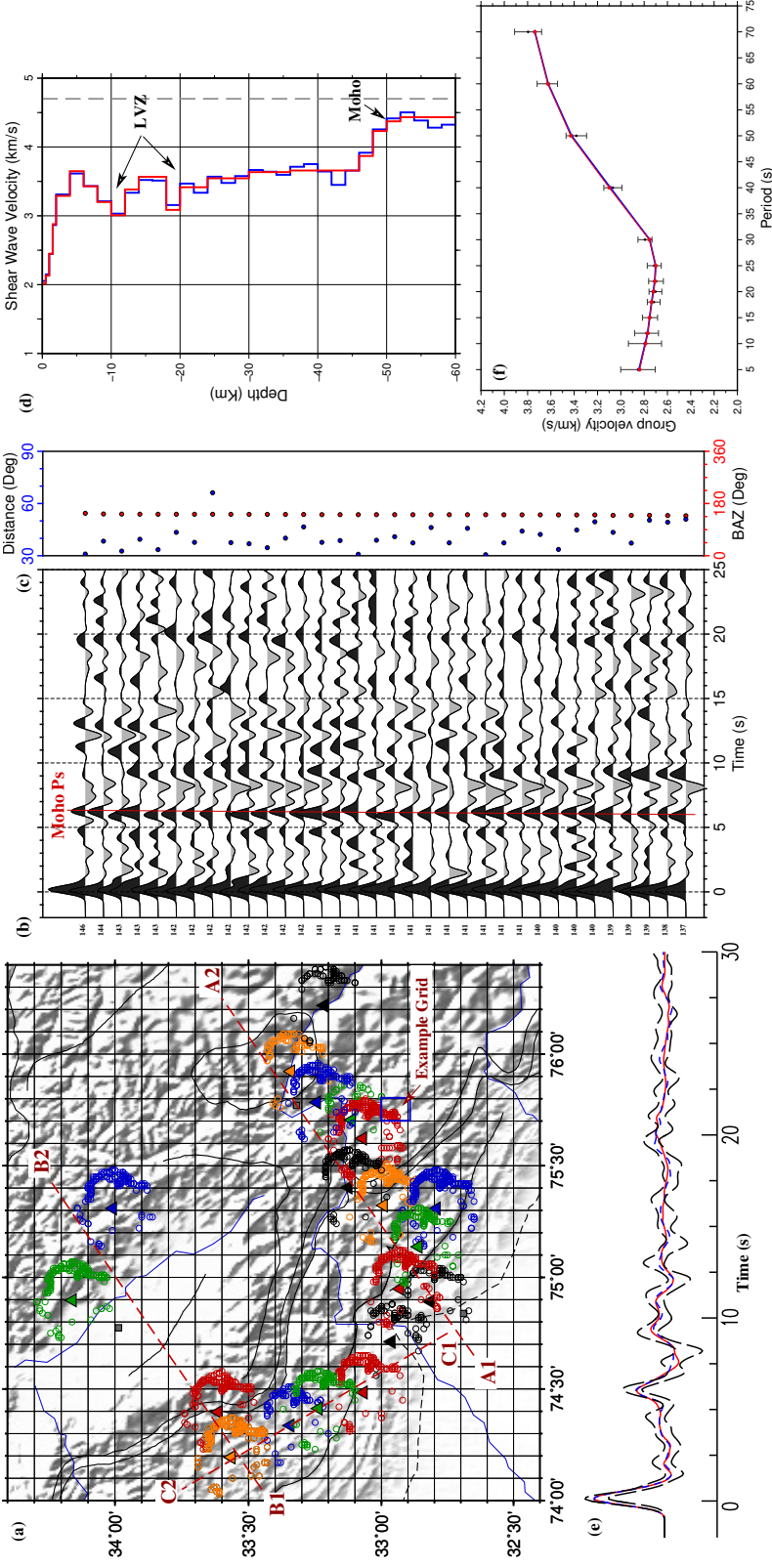


Figure 2. (a) Plot of Moho piercing points of R-RFs (colored circles) at a depth of 30 km. The color of the circles correspond to the station (colored triangles) at which the P-RF is calculated. P-RF stacks are calculated for the P-RFs within each 0.1° square grids shown on the map. Joint inversion of P-RFs and dispersion data is performed for each square grid. An example grid is marked on the map. Three P-RF profiles are marked as red dashed lines: A1-A2 (Fig 3), B1-B2 (Fig. 4) and C1-C2 (Fig. 5). (b) Individual P-RFs for the example grid in (a), calculated for Gaussian width 2.5 and plotted as a function of back-azimuth. (c) Plot of the distance and back-azimuth for individual P-RFs in (b). (d) V_s models obtained from the joint inversion of P-RFs and dispersion dataset. Blue is the thinly parameterized model from this study and red is the minimum layer model from Sharma et al. (2020). (e) $\pm 1 \sigma$ bounds of the stacked (average) P-RFs calculated from the individual ones in (b) is plotted as black dashed lines; and (f) Rayleigh wave fundamental mode group velocity dispersion data (Gilligan & Priestley, 2018) corresponding to the example grid in (a) is plotted as black error bars. Synthetic P-RFs in (e) and dispersion curve in (f), computed for the two joint inverted models in (d), are plotted in blue and red.

Further north the Moho Ps deepens to ~ 6.5 s beneath the Lesser Himalaya, and continues flat. It then shallows to ~ 6 s beneath the Higher Himalaya, before deepening to ~ 7 s beneath the Kishtwar Window and ~ 8 s beyond it. In the depth migrated 2D CCP stack, the Moho is observed as a strong positive arrival with an overall northeastward dip and undulations beneath the Higher Himalaya and Kishtwar Window (Fig. 3a). In the SW, the Moho is at a depth of ~ 45 km beneath the Shiwalik, ~ 50 km beneath the northern Sub-Himalaya, ~ 55 km beneath the Lesser Himalaya, 55–60 km beneath the Higher Himalaya and Kishtwar Window, and then dips sharply to ~ 70 km further NE. A deeper segment of the Moho at ~ 55 –60 km is observed beneath the Shiwalik at SMVD. This abrupt change in Moho depth and apparent southeastward dip, further to the north, indicate deviation from a uniform thickness Indian crust, under-thrusting the Himalaya. This variation is enhanced by along strike lateral variation in the structure. Moho depths obtained from station-wise joint inversion in narrow back-azimuth bins by Sharma (2020) closely match the Moho signal in the CCP stack (Fig. 3a,b).

The next significant phase in the Jammu–Kishtwar P-RF profile is the negative phase at ~ 1 s beneath the Shiwalik, which continues flat beneath the Lesser Himalaya and deepens to ~ 2 s beneath the Higher Himalaya, and ~ 3 s further north (Fig. 3c). From CCP profiles across other segments of the Himalaya (Schulte-Pelkum et al., 2005; Acton et al., 2011; Caldwell et al., 2013; Singer et al., 2017), we identify this as the signature of the Main Himalayan Thrust (MHT), a boundary which demarcates the under-thrusting Indian crust from the overriding Himalayan wedge. In the CCP stack, this phase is at a depth of ~ 8 km beneath the southernmost station (NGRT) in the Shiwalik, and deepens northeastward to ~ 10 km beneath the northern Sub-Himalaya (RAMN), having a gentle dip of $\sim 4^\circ$ (Fig. 3a). Beneath the Lesser Himalaya the MHT is flat at a depth of ~ 10 km. In this zone, the MKT, RT and MBT splay out of the MHT at steeper angles and are also marked by negative velocity change. Further north, beneath the Higher Himalaya, the MHT deepens from ~ 10 km to ~ 16 km within a distance of ~ 20 –25 km, dipping at ~ 13 – 17° . This marks a mid-crustal ramp on the MHT (also referred to as the MHT frontal ramp in this study). The MCT possibly splays out of the up-dip edge of this MHT ramp and steepen towards the surface. Beneath the Kishtwar window the MHT flattens at ~ 16 km and then deepens northeastward to ~ 20 km, beyond the northern edge of the Kishtwar window. Beneath the Kishtwar window a number of steeply dipping negative phases splay up-dip from the MHT. These are possible signatures of the

Lesser Himalayan Duplex (LHD), above and down-dip of the MHT mid-crustal ramp. The under-thrusting Indian crust (between the MHT and Moho) has an average thickness of ~ 40 km with marginal thickening beneath the Lesser Himalaya. The third most significant arrival in the CCP is a positive velocity change phase at a depth of ~ 30 km beneath the Shiwalik, which dips northwards and reaches a depth of ~ 45 km north of the Kishtwar window (Fig. 3a). We identify this as the mid-crustal boundary of the under-thrusting Indian crust. This mid-crustal interface is almost parallel to the Moho, and divides the Indian upper and lower crusts into thickness of ~ 25 km and ~ 15 km, respectively.

We plot 2D V_s profile (extracted from the 3D modeling) to compare the interfaces with the V_s velocities (Fig. 3b). The slowest V_s (< 3.0 km s $^{-1}$) are observed in the sediments of the Foreland Basin and Shiwalik, with maximum thickness of ~ 3 km. At depth of 8–10 km across the Foreland Basin, Sub- and Lesser-Himalaya is a gently NE dipping low velocity layer (LVL), which corresponds to the MHT in CCP stack profile. The dip of the LVL increases beneath the Higher Himalaya and continues further NE reaching a depth of ~ 20 km. The V_s within the LVL increases towards the hinterland from 3.1 to 3.3 km s $^{-1}$. The Higher Himalaya has higher V_s of 3.4–3.5 km s $^{-1}$, compared to its south and above the LVL, attesting to crystalline rocks. Below the MHT, between depths of ~ 10 and 60 km, the V_s contours are mostly sub-horizontal and dips towards the hinterland. Moho depths from individual station back-azimuth binned P-RF joint inversion (Sharma, 2020) lie within V_s contours of 4.1–4.4 km s $^{-1}$, with signatures of laterally varying Moho depth beneath SMVD and RAMN. Comparison of the mid-crustal discontinuity from CCP stack with the V_s model shows its correspondence to V_s contours of ~ 3.7 –3.8 km s $^{-1}$. Among other phases in the P-RF spatial stack, we observe a coherent positive P_s phase within ~ 1 s of the MHT negative phase (Fig. 3c). This is produced from the positive velocity gradient below the LVL. The ~ 4 s negative phase between distances of 60 km and 160 km along the profile is a reverberation from the shallow structure.

The second 2D profile is oriented SW-NE across the Pir-Panjal Ranges, Kashmir Valley and Zaskar Ranges (B1–B2 Fig. 2a). This straddles the northern Sub-Himalaya (MEND), Lesser Himalaya (BUFL), and Kashmir Valley Tertiary sediments overlying the Tethyan Himalaya (HARW and PAHL). P-RFs have a distinct Moho P_s arrival at ~ 7 s beneath the northern Sub-Himalaya, which shallows NE to ~ 6 s beneath the Kashmir Valley and then deepens further north to ~ 7.5 s beneath the Tethyan Himalaya (Fig. 4c).

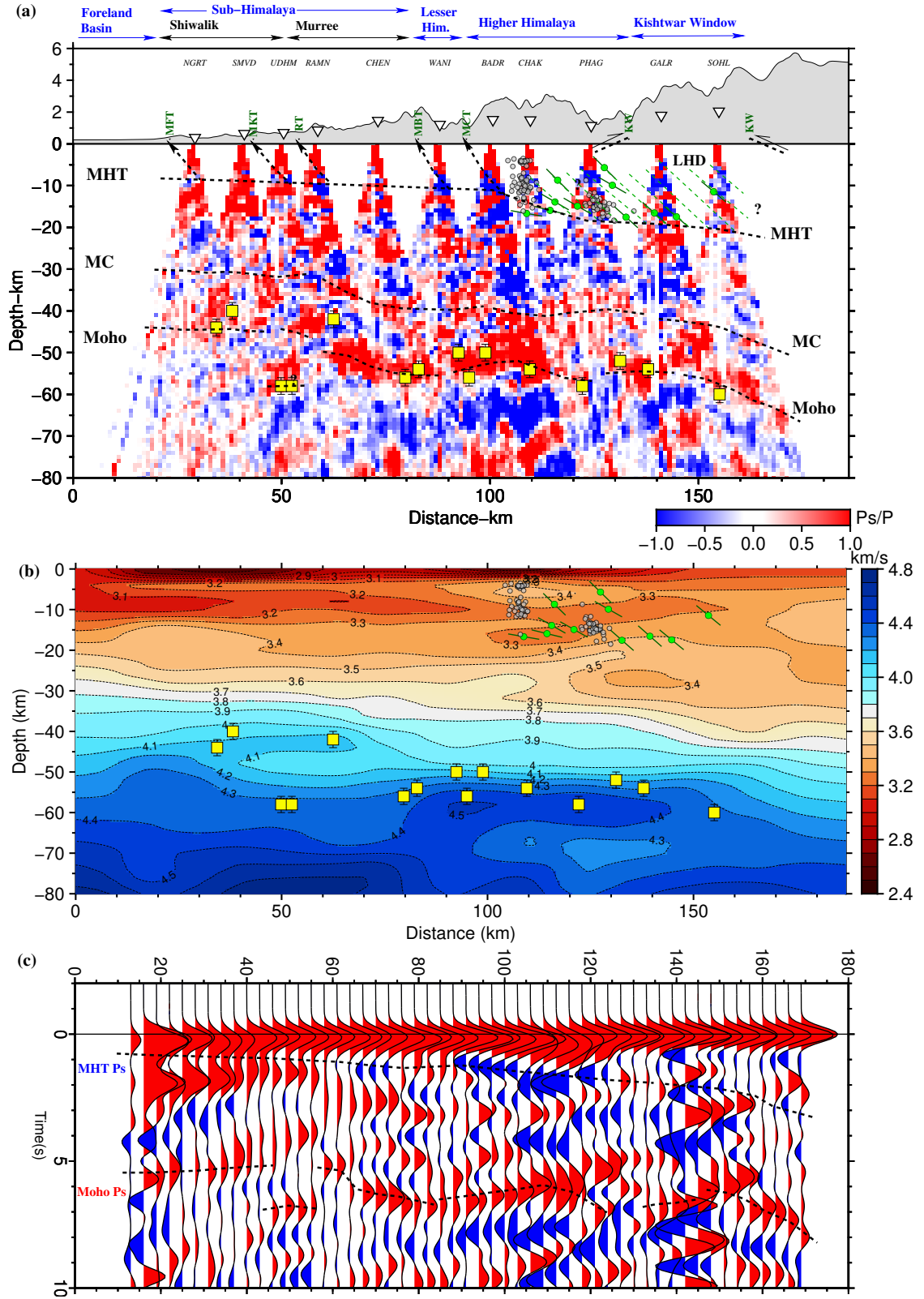


Figure 3. Caption on next page.

Figure 3. (previous page) (a) CCP receiver function image along profile A1–A2 (Fig. 1a). Positive Ps amplitude is red and negative amplitude is blue. MHT, mid-crustal discontinuity and Moho are marked by black dashed lines. Subsurface disposition of the mapped thrusts/faults are plotted as black dashed line with an arrow head and labeled in green above. Stations are plotted as inverted white triangles and labeled by station code on top of the plot. Earthquakes from Paul et al. (2018) are plotted on the CCP as grey circles and from O’Kane et al. (2022) as green circles, with the fault plane dip plotted as black lines. Moho depths obtained from joint inversion (this study) are plotted as yellow squares with error bars in black. (b) Plot of V_s model, along the same profile, obtained from inversion at node points of the 2D grid. (c) P-RF stacks (binned every 3 km) plotted along the same profile. Positive Ps amplitude is red and negative amplitude is blue. MHT and Moho Ps phases are marked by black lines.

Our network has a gap between the central Pir-Panjal Ranges and the central Kashmir Valley. Moho depth in this gap is taken from the P-RF study of Mir et al. (2017). In the CCP, the Moho is at a depth of ~ 60 km beneath the northern Sub-Himalaya and displays an undulatory nature with distinctive southward dip beneath the Pir-Panjal Ranges (Fig. 4a). Beneath the Kashmir Valley the Moho is flat at ~ 55 km (Mir et al., 2017) and then dips NE reaching a depth of ~ 65 km beneath the Zaskar Ranges. The MHT is marked by a negative velocity change interface and appears flat at ~ 10 km beneath the Pir-Panjal Ranges and the Kashmir Valley. The MHT mid-crustal (frontal) ramp observed in the Jammu–Kishtwar profile, appears to be underneath the Zaskar Ranges, where it deepens to ~ 15 km. The Zaskar Shear Zone (ZSZ), equivalent of the Southern Tibetan Detachment (STD) mapped in the Nepal Himalaya, splays up-dip from the MHT frontal ramp. Albeit the gap in stations/data from this profile, we suggest that the MBT, MCT and BF splays up-dip from the MHT. The mid-crustal interface is observed at a depth of ~ 30 km beneath the northern Sub-Himalaya and the Pir-Panjal Ranges, possibly stays flat beneath the Kashmir Valley and dips northwards beneath the Zaskar Ranges to a depth of ~ 45 km. From the V_s profile we observe a thin layer (< 2 km) of slow V_s sediments (< 3.0 km s $^{-1}$) beneath the northern Sub-Himalaya (Fig. 4b). A flat LVL at ~ 10 km depth, with V_s of 3.2–3.3 km s $^{-1}$, marks the MHT beneath the Sub-Himalaya. The V_s within the LVL increases marginally to 3.4 km s $^{-1}$ beneath the Kashmir Valley and dips NE beneath the Zaskar Ranges. The Kashmir Valley is underlain by higher V_s compared to the Sub-Himalaya and the Pir-Panjal Ranges. Similar to the Jammu–Kishtwar

profile, the V_s contours within the Indian crust (below the LVL) are undulatory and dip gently towards the hinterland. Moho depths from joint inversion (Sharma, 2020) corresponds to V_s of 4.2–4.4 km s⁻¹. There is a down-warping of the 4.3 km s⁻¹ V_s contour beneath the Pir-Panjal Ranges. This possibly indicate a thicker crust, with a high V_s (~ 4.2 km s⁻¹) lower crustal layer beneath the high ranges. However, this signature is not evident in the CCP stack. The mid-crustal discontinuity corresponds to V_s contours of ~ 3.7 – 3.8 km s⁻¹.

The third 2D profile is oriented SSE-NNW across the Sub-Himalaya (C1–C2 Fig. 2a). The southern end of the profile is NW of Jammu in the Foreland Basin sediments and extends to the foothills of the Pir-Panjal Ranges. P-RFs from five stations are used in this profile, of which AKNR and SUND are located on the Shiwalik and TAPN, RAJU and MEND are on the northern Sub-Himalaya. The Moho Ps phase is the strongest arrival in the P-RFs. It is at ~ 6 s beneath AKNR, deepens to ~ 7.5 s beneath SUND, shallows marginally to ~ 7 s beneath TAPN and RAJU, and finally dips gently beneath MEND (Fig. 5c). The MHT negative phase is flat at ~ 1 s up to 90 km along the profile, after which it dips gently to ~ 2 s. In CCP stack the Moho is undulatory with strong northward dip beneath the Shiwalik (AKNR) and northern Sub-Himalaya (MEND) (Fig. 5a). In between the Moho flattens and dips southward. The depth to the Moho varies from ~ 50 km to ~ 65 km, with the deepest Moho beneath SUND and north of MEND. The mid-crustal discontinuity is marked by a positive phase in the CCP. It displays a similar undulatory geometry as the Moho and lies between ~ 35 km to ~ 45 km. The MHT is the shallow negative phase in the CCP. It is observed to be flat at ~ 6 – 8 km beneath the Shiwalik and ~ 10 – 12 km beneath the northern Sub-Himalaya, with possible gentle dipping segments beneath SUND and MEND. The KT and MFT splays up-dip from the MHT. The V_s model shows low V_s (< 3 km s⁻¹) sedimentary layer beneath the Sub-Himalaya, having thickness of ~ 3 km in the south and thinning northward (Fig. 5b). The MHT is marked by the LVL with V_s of 3.1–3.2 km s⁻¹, and dipping gently towards the NW. The joint inversion Moho depths (Sharma, 2020) lie between V_s contours of 4.2–4.4 km s⁻¹, both displaying similar undulatory nature of the Moho observed in the CCP. The mid-crustal discontinuity corresponds to V_s contour of 3.7–3.8 km s⁻¹. The thickened lower crust beneath SUND has a high V_s (~ 4.1 – 4.2 km s⁻¹) ~ 10 km layer at its base.

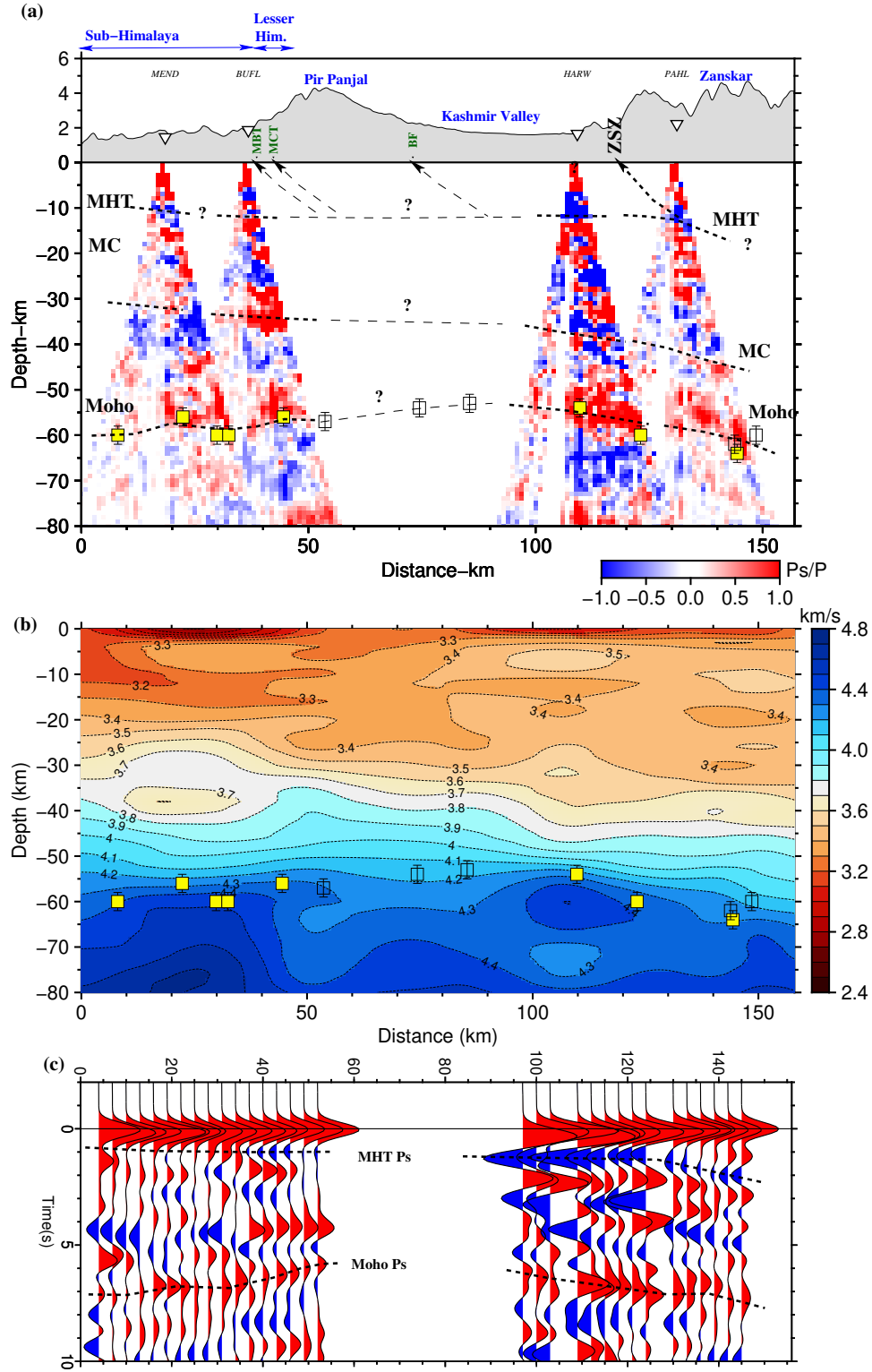


Figure 4. Caption on next page.

Figure 4. (previous page) Plot for profile B1–B2 (Fig. 1a). (a) CCP receiver function image. Moho depth from (Mir et al., 2017) from the Kashmir Valley are plotted as white squares. (b) Plot of V_s model. (c) Plot of radial receiver function stacks. Rest of the figure caption is same as figure 3.

Next, we study the lateral and depth variations in absolute V_s and V_s anomalies for the crust (0–40 km) using 2D maps (Fig. 6). The absolute V_s are averaged over depth ranges of 10 km. The V_s anomalies are calculated as percentage deviation from the average V_s for the depth range. The shallowest map is for depth range of 0–10 km. This mainly samples the sedimentary layers of the Himalayan Foreland Basin and the Himalayan wedge (Fig. 6a,b). The V_s varies from $\sim 2.8 \text{ km s}^{-1}$ to $\sim 3.4 \text{ km s}^{-1}$, with increasing V_s towards the hinterland (Fig. 6a). This indicates thinning of sedimentary layers and presence of meta-sediments in the Lesser and Higher Himalaya. This was also observed in the 2D profiles. The slowest (and possibly the thickest) sedimentary layers ($V_s < 3.0 \text{ km s}^{-1}$) are present in the Shiwalik (A1 in Fig. 6b) and in the Higher Himalaya, between the MCT reentrant and the Kishtwar Window (A2 in Fig. 6b). These correspond to negative V_s anomalies of $\sim 8\text{--}10\%$. The Pir-Panjal Ranges, Kashmir Valley and Zaskar Ranges have increasing positive V_s anomalies. The active Reasi Thrust (Gavillot et al., 2016) marks the transition between negative to positive V_s anomaly (A3 in Fig. 6b). V_s maps for depths 10–20 km sample around the MHT zone. This includes the top of the under-thrusting Indian crust in the SW and the base of the Himalayan wedge in the NE (Fig. 6c,d). This is due to flexural bending of the under-thrust Indian crust and hinterlandward increase in Himalayan wedge thickness. Increase in V_s is observed across-arc from foreland to hinterland (SW–NE), and along-arc from Kishtwar Himalaya to Kashmir Valley (SE–NW). V_s maps for depth range of 20–30 km samples the Indian middle-crust in the south, beneath the Foreland Basin; and the under-thrusting (gently dipping) Indian upper-crust beneath the Higher Himalaya (Fig. 6e,f). The increase in V_s occurs in the reverse direction (i.e. hinterland to foreland) compared to the shallower map. A higher velocity feature is observed orthogonal to the strike of the Himalayan thrust sheets. This is aligned along the reentrant of the MBT and MCT up to the Kishtwar window (A4 in Fig. 6e). This lies below the low V_s anomalies at shallower depth (0–10 km). For 30–40 km depth range, the V_s varies from $3.4\text{--}3.5 \text{ km s}^{-1}$ beneath the Tethyan Himalaya. The V_s increases to $3.5\text{--}3.8 \text{ km s}^{-1}$ beneath the Higher and Lesser Himalaya, and $3.8\text{--}4.0 \text{ km s}^{-1}$

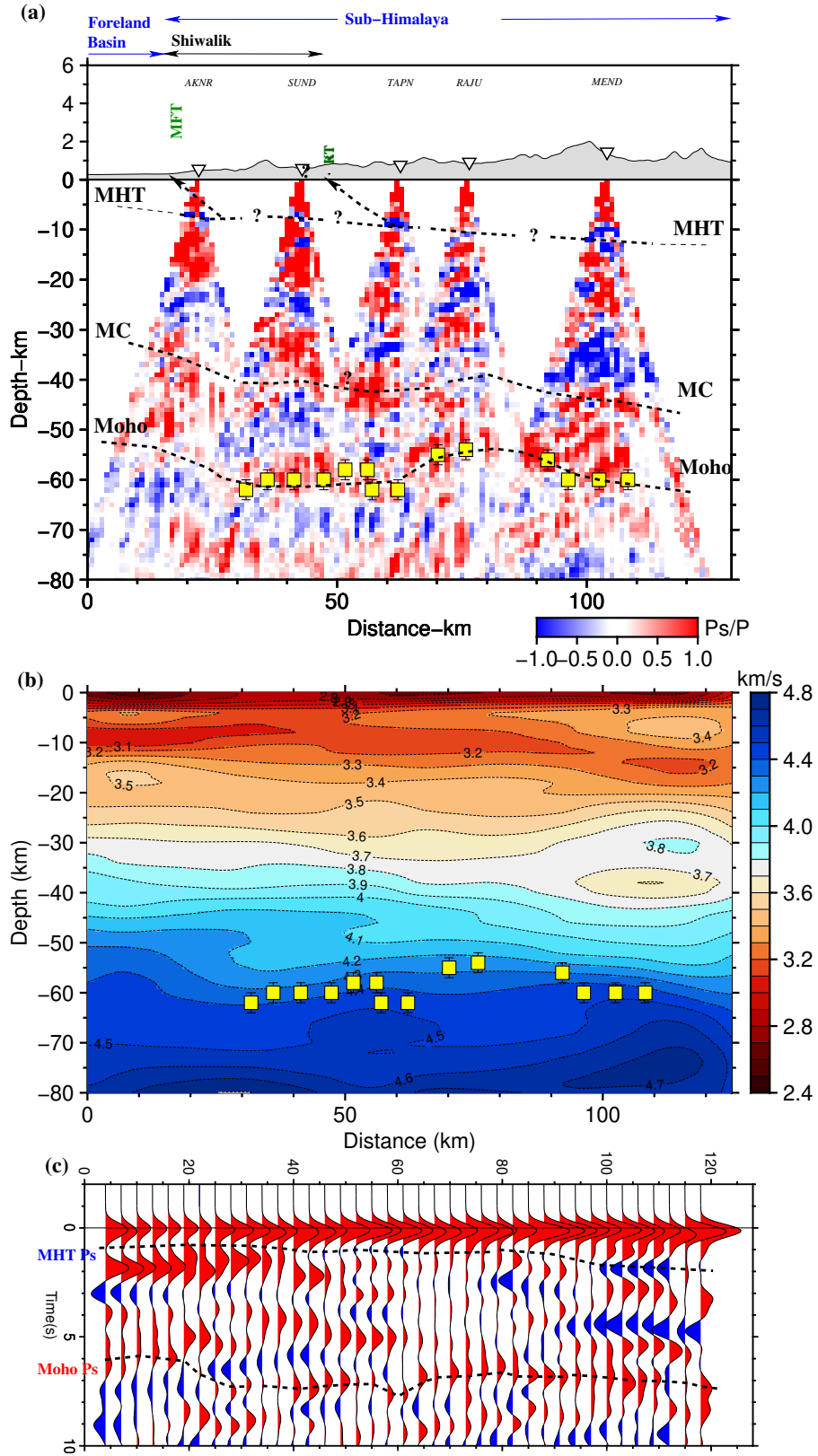


Figure 5. Caption on next page.

Figure 5. (previous page) Plot for profile C1–C2 (Fig. 1a). (a) CCP receiver function image. (b) Plot of V_s model. (c) Plot of radial receiver function stacks. Rest of the figure caption is same as figure 3.

beneath the Sub-Himalaya and Foreland Basin (Fig. 6g). This decreases in V_s towards the hinterland is due to sampling of the faster lower Indian crust beneath the foreland and marginally slower mid-to-lower crust beneath the Himalaya. This lateral variation is also observed in the V_s anomaly map (Fig. 6h).

Finally, we present 2D maps of the average crustal V_s and depth to the Moho beneath the J&K Himalaya (Fig. 7). The average crustal V_s varies between $\sim 3.4 \text{ km s}^{-1}$ and 3.65 km s^{-1} (Fig. 7a). Slowest average V_s ($3.4\text{--}3.5 \text{ km s}^{-1}$) is observed in the sedimentary layers of the Sub-Himalaya. The region following the reentrant of the MFT, MBT and MCT, up to the Kishtwar window also have slow V_s . Embedded between the low average V_s north of the MCT reentrant and the Kishtwar Window is an average high V_s linear feature, oriented NW-SE (A5 in Fig. 7a). Similar low-to-high V_s transition is observed immediately NE of the Reasi Thrust (A6 in Fig. 7a). Significant higher average V_s ($\sim 3.55\text{--}3.65 \text{ km s}^{-1}$) is observed beneath the Pir-Panjal Ranges, Kashmir Valley and the Zaskar Ranges. These regions have higher V_s compared to the eastern Jammu-Kishtwar Himalayan segment. The Moho from our 3D V_s model is chosen as a boundary with average V_s of 4.3 km s^{-1} in the uppermost mantle (Fig. 7b). This is guided by the match between the joint inversion derived Moho depth (Sharma, 2020) and the V_s contours in the 2D profiles (Figs. 33b, 4b and 5b). This choice is supported by the close correspondence between the Moho depths of Sharma (2020) (colored circles) and the Moho depth contours in our 3D model (Fig. 7b). To the first order, the Moho is observed to dip gently towards the hinterland, with its depth varying from $\sim 45 \text{ km}$ (beneath the foreland in the SW) to $\sim 70 \text{ km}$ (beneath the Higher and Tethyan Himalaya in the NE). Laterally, significant differences are observed in Moho depth and geometry between the Jammu-Kishtwar Himalaya and the Kashmir Valley. Regions with slowest V_s , beneath the Shiwalik and the reentrant of the MFT, MBT and MCT (up to the Kishtwar Window) are marked by the shallowest Moho. The Moho abruptly deepens north of the Reasi Thrust by $\sim 10 \text{ km}$. This was also observed in the CCP stack profile as a

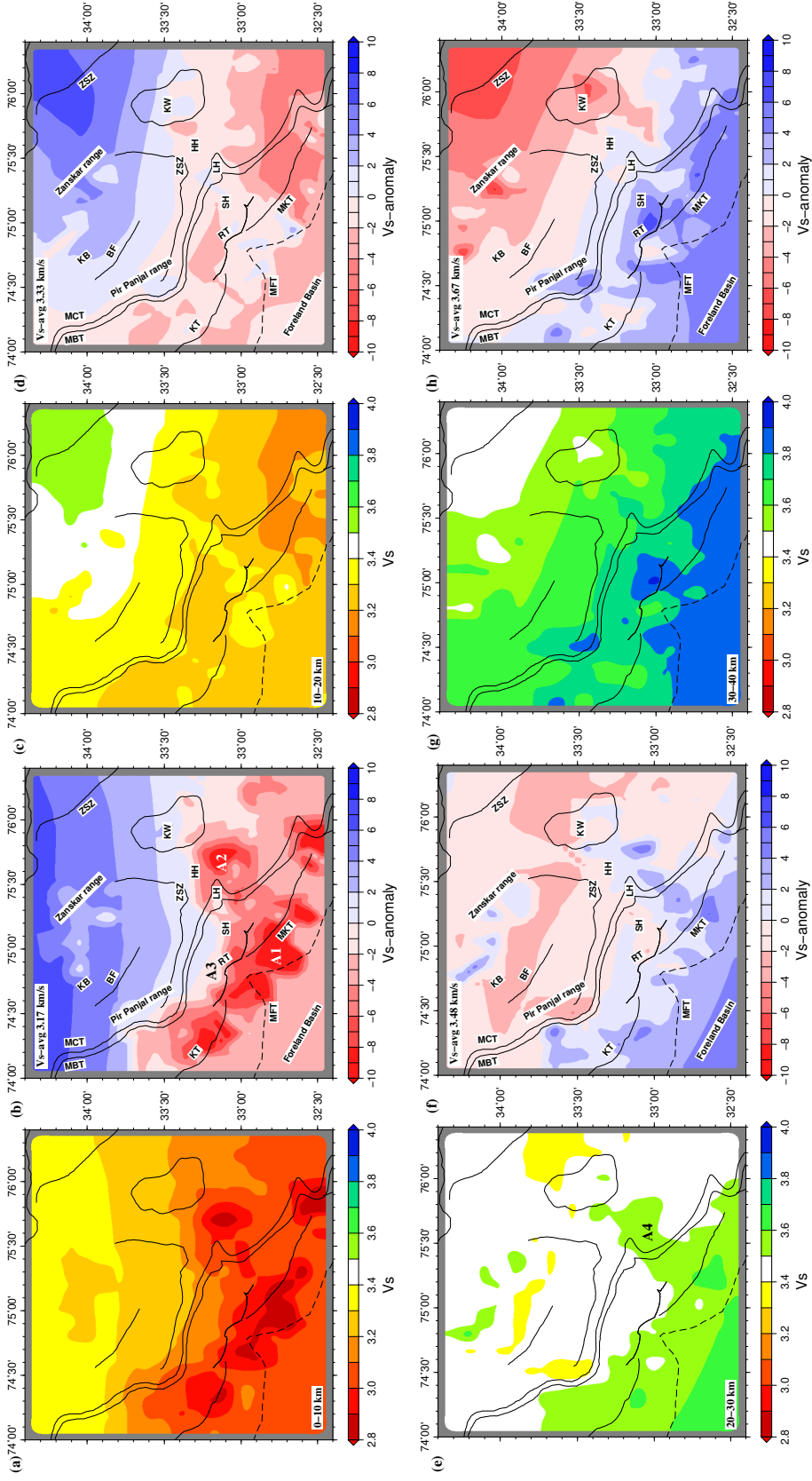


Figure 6. (a) Map of average V_s for depth range of 0–10 km, obtained from inversion at node points of the 2D grid. (b) V_s anomaly map corresponding to (a). (c) Average V_s map for depth range 10–20 km, and (d) corresponding V_s anomaly map. (e) Average V_s map for depth range 20–30 km, and (f) corresponding V_s anomaly map. (g) Average V_s map for depth range 30–40 km, and (h) corresponding V_s anomaly map.

deeper Moho segment (Fig. 3a). The Pir-Panjal Ranges and Kashmir Valley has ~ 15 km deeper Moho compared to the Jammu-Kishtwar Himalaya.

5 Discussion

5.1 Geometry of the MHT and structure of the Himalayan wedge

The Main Himalayan Thrust (also referred to as the basal decollement of the Himalayan mountains) marks the boundary between the top of the under-thrusting India crust and the base of the overriding Himalayan wedge. All or most of the present day convergence across the Himalaya is accommodated by slip on the MHT (Stevens & Avouac, 2015). The shallow up-dip segment of the MHT deforms seismogenically through cycles of frictional locking and failure in thrust-fault earthquakes, while the deeper down-dip segment creeps aseismically. The transition from locked-to-creep occurs through a zone of tapered slip (unlocking zone), which have been mapped to coincide with a mid-crustal ramp on the MHT beneath Sikkim (Acton et al., 2011), Nepal (Nábělek et al., 2009) and Garhwal Himalaya (Caldwell et al., 2013). The MBT, MCT and other major faults within the Himalayan orogen splay up-dip from the MHT. Growth of the Himalayan orogen, over geological timescales, is controlled by the evolution of the MHT and its splay faults. Therefore, knowledge of the three-dimensional structure of the MHT holds key to both geological and tectonic processes in the Himalaya.

Thrust faulting on the MHT juxtaposes deeper rocks, with higher velocity and density, over shallower rocks, resulting in negative impedance-contrast at the interface. Additionally, at shallow depth, the top of the down-going Indian crust entrains low-velocity fluid-saturated sediments of the Indo-Gangetic Foreland Basin, enhancing the low velocity associated with the MHT (blue in CCPs). We observe remarkable difference in the disposition of this MHT LVL between the Jammu-Kishtwar Section and the Kashmir Valley section and explore its across and along arc transitions. In both sections the MHT is gently dipping ($\sim 4^\circ$) beneath the Sub-Himalaya, ranging in depth from 5–6 km to ~ 10 km. Beneath the Kishtwar Higher Himalaya it steepen significantly (dip ~ 13 – 17°) in the form of a MHT mid-crustal (frontal) ramp, and reaches a depth of ~ 20 km beyond the Kishtwar Window. The aftershocks of the 2013 Kishtwar earthquake (Paul et al., 2018) are concentrated on and above the edges of the ramp, indicating a zone of stress accumulation and possibly a locked-to-creep transition. Along strike to the NW, beneath the

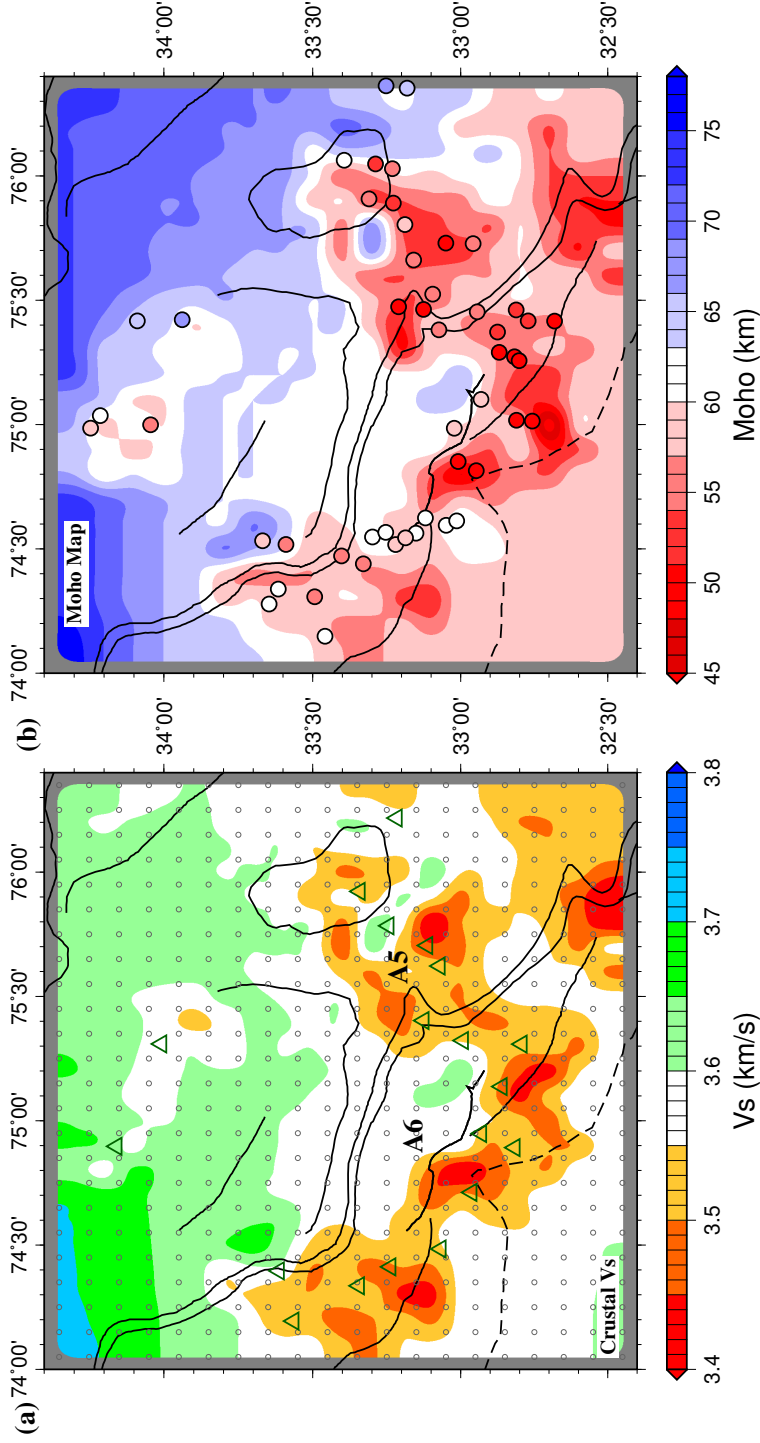


Figure 7. (a) Plot of lateral variation in average crustal V_s , obtained from the inversion at node points of the 2D grip. Small circles represent these node points and green triangles are stations. (b) Plot of Moho depth obtained from the V_s model in (a) corresponding to V_s 4.3 km s^{-1} . The colored circles representing Moho depth obtained from joint inversion of receiver function clusters with dispersion data. Note the match in Moho depths obtained from the two analysis.

Kashmir Valley, the MHT is flat at ~ 10 km without clear signatures of a mid-crustal ramp. If at all present, the ramp could be beyond the Valley, beneath the Zaskar Ranges, where the MHT LVL starts to steepen. However, this lies at the northern edge of our network to provide a conclusive image. A set of steeply-dipping negative-impedance boundaries are observed in the Kishtwar Higher Himalaya, above the MHT mid-crustal ramp. These appear like slivers of ~ 5 km thickness, and align with the fault planes of moderate earthquakes (O’Kane et al., 2022). We infer this to be the Lesser Himalayan Duplex (LHD) beneath the Kishtwar Window, bound by the MHT sole-thrust and the MCT roof-thrust. In the inter-seismic period, the convergence across the Himalayan arc accumulates stress on and above the MHT unlocking zone, resulting in micro-to-moderate seismicity (Ader et al., 2012). The LHD coincides with this zone and provides pre-existing weak planes (thrust horses) on which the seismicity possibly occurs. The match between the moderate earthquake fault-plane dip and the steeply dipping planes attest to this brittle deformation of the LHD within the Himalayan wedge, thereby illuminating its structure. Such a LHD structure is not observed in the CCP beneath the Kashmir Valley segment.

To understand the along-arc transition of the MHT from a deeper boundary (with LHD structure above) in the Kishtwar Window, to a shallower flat-boundary in the Kashmir Valley, we constructed two V_s profiles of the intervening region (Fig. 8). The dipping V_s contours match the distribution of the earthquakes (Paul et al., 2018) confirming the presence of a lateral ramp on the MHT. This lateral ramp dips to the SE and connects the shallower segment of the MHT beneath the Kashmir Valley to the deeper segment beneath the Kishtwar Window. The lateral ramp continues up-dip and down-dip on the MHT, and splay faults above the lateral ramp form the reentrant structures of the MFT, RT, MBT and MCT seen in map view (Figs. 1b and 8c). Across-arc anomalies A2 and A5 (Figs. 6b and 7a) are signatures of this MHT lateral ramp. The partitioning of convergence between the range front (MFT beneath SMA) and the RT, within the Sub-Himalaya, could be controlled by this 3D structure of the MHT. Furthermore, the MHT frontal and lateral ramps intersect immediately south of the Kishtwar Window to form a complex zone of locked-to-creep transition. The 2013 Kishtwar earthquake aftershocks are concentrated on and above these two intersecting edges (Fig. 8d). In the Kashmir Valley segment, this locked-to-creep transition appears to lie further to the north beneath the Tethyan Himalaya (Zaskar Ranges). These findings have significant im-

plications for seismic hazard of the J&K Himalaya and models of long-term shortening across the NW Himalayan arc as discussed below.

The presence of the MHT lateral ramp introduces lateral heterogeneity on the MHT and could influence the size and/or rupture pattern of future mega-thrust earthquakes. The $\sim 11 \text{ mm yr}^{-1}$ arc-normal convergence across the Kashmir Himalaya (Schiffman et al., 2013) has accumulated $\sim 5 \text{ m}$ of potential slip within the $\sim 100 \text{ km}$ wide frictionally-locked zone on the MHT (between the range-front MFT and the MHT mid-crustal (frontal) ramp with concentration of moderate-sized seismicity). Assuming that this entire elastically stored energy is released in a future mega-thrust earthquake on the MHT, the along-arc length of the rupture will determine the size of the earthquake and its associated hazard. Several possible rupture scenarios could be worked out and incorporated in quantification of ground shaking. These would range from end-member scenarios where (a) the lateral ramp on the MHT acts as an asperity barrier and results in a relatively smaller $M_w \sim 7\text{--}7.5$ earthquake (depending on partial or complete rupture); or (b) the mega-thrust ruptures the entire length of the MHT locked zone in a relatively larger $M_w 8+$ earthquake, and the lateral ramp modulates the rupture speed as observed in the 2015 Gorkha earthquake (Kumar et al., 2017).

The difference in depth and slope on the MHT between the Jammu-Kishtwar Himalaya and the Kashmir Valley is associated with remarkably different wedge structures. The presence of the steeply dipping MHT mid-crustal (frontal) ramp and the LHD beneath the Kishtwar Window confirms the inference made from balanced cross-section that the arc-perpendicular shortening of the Jammu-Kishtwar Lesser and Higher Himalaya to have occurred through discreet accretion of thrust horses along the ramp. The CCP images, and moderate earthquake fault plane dip, provides additional constraints on the dip and thickness of these stacked sheets within the LHD. On the other hand the Kashmir Valley is underlain by a flat MHT with no evidence of a MHT ramp or an LHD structure beneath it. The arc perpendicular shortening across the Pir-Panjal to the Zaskar Ranges was most probably accommodated by frontal accretion (Yu et al., 2015). From the structure and the seismicity, there is no evidence of any active out-of-sequence thrust in either segments of the J&K Himalaya. The lateral difference in style of convergence was possibly guided by the presence of the NW syntaxis and the westward increase in width of the Sub-Himalaya.

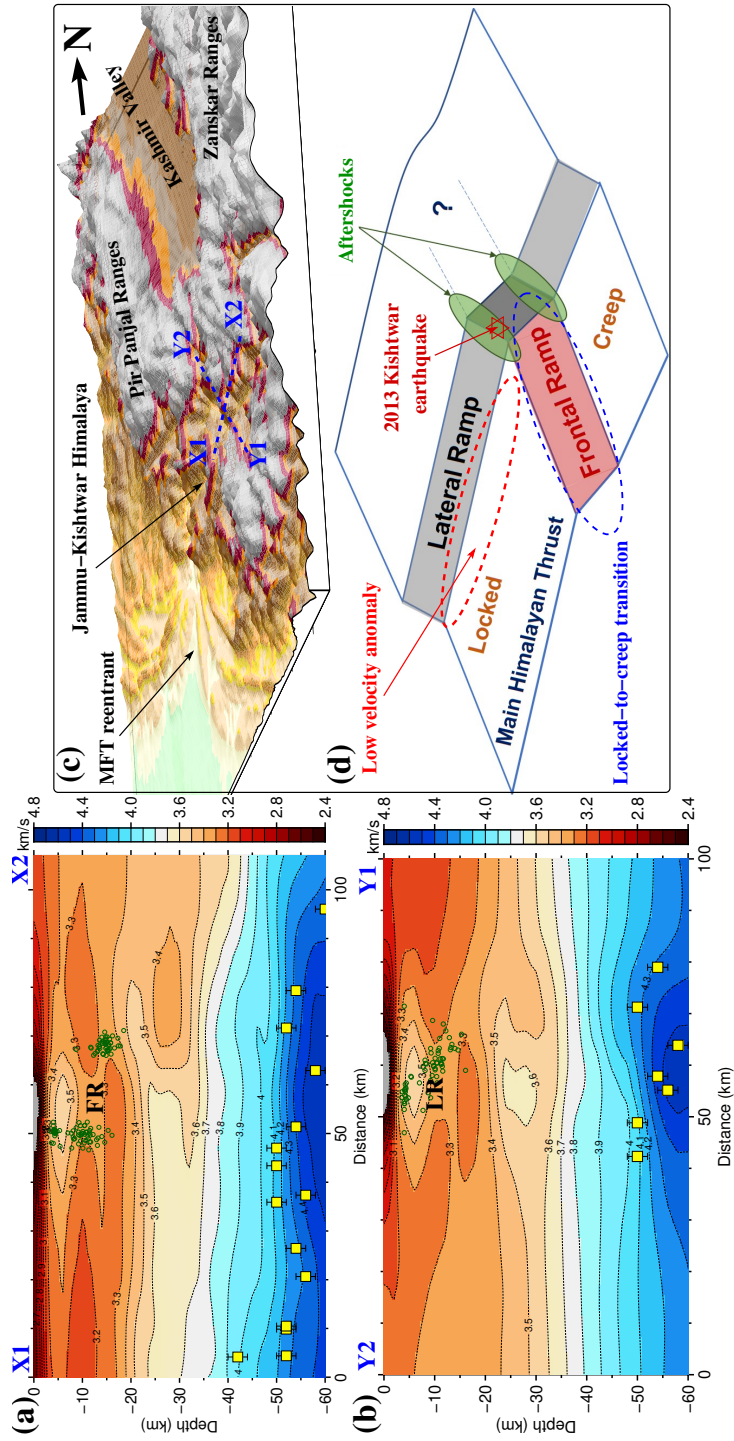


Figure 8. Plot of V_s profiles (a) X1–X2 (Fig. 1d) across the Himalayan arc, and (b) Y1–Y2 along the Himalayan arc, in the Jammu-Kishtwar Himalaya, focusing on the MHT ramps. Aftershocks of the 2013 Kishtwar earthquake, taken from Paul et al. (2018), are plotted as green circles on both profiles. The MHT mid-crustal (frontal) ramps lies between the two clusters of aftershocks in (a) and is along the steep dipping V_s contours. The lateral ramps in (b) is aligned with the dipping distribution of aftershocks. (c) Perspective view of the Kishtwar Himalayan tomography with the two profiles marked on top. (d) Schematic illustrating the disposition of the MHT ramps and the associated seismicity.

5.2 Crustal thickness variations and geometry of the Indian Moho

The Moho depth beneath the Pir-Panjal Ranges, the Kashmir Valley and the Zaskar Ranges is deeper by $\sim 10\text{--}15$ km compared to the Jammu-Kishtwar Himalaya (Fig. 7b). This region of deeper Moho is associated with shallower and flat MHT, which reveals a thicker under-thrust Indian crust beneath the Kashmir Valley region. From gravity anomalies it is known that the northern Indian cratonic crust is in isostatic equilibrium. Following this we assume that the presently under-thrust Indian crust beneath the J&K Himalaya was also in isostatic equilibrium before diving beneath the Foreland Basin sediments. The modeled lateral variation in the Indian crustal thickness, from $\sim 45\text{--}50$ km beneath the Kashmir Valley to $\sim 40\text{--}45$ km beneath the Kishtwar Himalaya, is an inherited characteristic of the cratonic Indian crust. Its undulatory top surface controls the present day geometry of the MHT, including the lateral ramp. Additionally the region of thicker Indian crust has higher average V_s (Fig. 7a), which is a combined effect of higher V_s in the thicker cratonic crust due to possible mafic under-plating, and the thinner sedimentary layers overlying it. The flexural bending of the under-thrust crust is evident in the long-wavelength increase in Moho depth towards the NE direction from $\sim 45\text{--}50$ km to $\sim 65\text{--}70$ km. We also suggest that the MFT, MBT and MCT reentrant, observed in the Jammu-Kishtwar window, is a surface expression of the MHT lateral ramp and southward dipping Himalayan topography (Fig. 8c,d).

6 Conclusions

Teleseismic waveforms from 20 JAKSNET stations have been used to model the 3D seismic velocity structure of the J&K Himalaya. P-RF spatial and CCP stack profiles are computed across the Himalayan arc through Jammu-Kishtwar segment (E) and Pir-Panjal-Kashmir Valley-Zaskar Ranges (W). Joint inversion of P-RFs with Rayleigh wave group velocity dispersion data is performed for 2D grids at 0.1° intervals. These provide the first comprehensive image of the crust and uppermost mantle structure beneath J&K Himalaya and highlights the across and along arc lateral variations. The main conclusions of this study are as follows:

- 2D profiles of P-RF spatial and CCP stacks reveal increasing crustal thickness from the foreland to the hinterland, and an under-thrust Indian crust beneath the J&K Himalaya. The bottom and top of the under-thrust crust is marked by positive

and negative impedance contrast boundaries, corresponding to the Moho and MHT, respectively. To the first order the Moho dips gently towards the hinterland. It is modeled at a depth of ~ 45 km beneath the Shiwalik Himalaya and deepens to ~ 70 km beneath the Higher and Tethyan Himalaya. The MHT juxtaposes deeper crustal rocks over shallower ones, and entrains fluid saturated Foreland Basin sediments, resulting in a LVL. The MHT LVL has a flat-ramp geometry with gently dipping ($\sim 4^\circ$) flat segment beneath the Sub and Lesser Himalaya, at 6–10 km depth. A steeper mid-crustal (frontal) ramp (dip ~ 13 – 17°) lies beneath the Kishtwar Higher Himalaya and Zaskar Ranges, at ~ 10 – 16 km depth.

- The structure across the Jammu-Kishtwar Himalayan segment in the east is distinctly different from the western segment across Pir-Panjal Ranges, Kashmir Valley and Zaskar Ranges. The Moho beneath the RT in Sub-Himalaya has a lateral depth variation of ~ 10 – 15 km, and has SW dipping segments beneath the Lesser Himalaya and Kishtwar Window. A LHD structure is imaged beneath the Kishtwar Window, bound between the MHT sole thrust and MCT roof thrust. The LHD horses dip at high angle to the bounding structure, align with earthquake fault plane dip and have average thickness of ~ 5 km. The under-thrust Indian crust, bound between the MHT and Moho, have a thickness of ~ 40 – 45 km beneath the Jammu-Kishtwar segment. On the other hand the Moho is at a depth of ~ 60 km beneath the northern Sub-Himalaya and Lesser Himalaya along the southern edge of the Pir-Panjal Ranges. It shallows to ~ 55 km beneath the Kashmir Valley with SW dipping segment. Further north it gently dips towards NE and reaches a depth of ~ 65 km beneath the Zaskar Ranges. The MHT is flat at ~ 10 km across the entire Kashmir Valley segment and have no signature of LHD structure. The MHT mid-crustal (frontal) ramp lies beneath the Zaskar Ranges, at the edge of our network. The Indian crust is ~ 45 – 50 km thick beneath the Kashmir Valley segment of the Himalaya, marginally thicker than the eastern Jammu-Kishtwar segment.
- The under-thrust Indian crustal thickness increase from east to west, beneath the J&K Himalaya, is associated with increase in Moho depth and average crustal V_s . For an isostatically balanced Indian crust, this thickness variation results in a deeper MHT in the east compared to the west. The E-to-W transition occurs through a lateral ramp on the MHT. Splay faults above the lateral ramp outcrop as reentrant. The aftershocks of the 2013 Kishtwar earthquake concentrate on the inter-

section of the frontal and lateral ramps beneath the Kishtwar Higher Himalaya. This possibly marks the down-dip locked-to-creep transition on the MHT. This transition to the west is suggested to lie beneath the Zaskar Ranges.

- This study provides the first sub-surface image of the LHD beneath the Kishtwar Himalaya. The geological arc-perpendicular shortening of the Jammu-Kishtwar Lesser and Higher Himalaya had occurred through discrete accretion of thrust horses above the MHT mid-crustal (frontal) ramp, which are illuminated by moderate magnitude earthquakes. Whereas, the Kashmir Valley is underlain by a flat MHT, and the arc-perpendicular shortening across the Pir-Panjal to Zaskar Ranges, most probably, occurred by frontal accretion.

Open Research Section

Data used for this study are P-RFs computed from teleseismic earthquakes and are shared through the public data repository: <https://doi.org/10.5061/dryad.hhmgqkn4>

Acknowledgments

This research and the establishment of JAKSNET had been funded through the following grants: (a) UK-IERI Thematic Partnership Award (2012-2014) between IISER Kolkata and University of Cambridge (Grant No. IND/2011-12/EDU-UKIERI/156); (b) UGC-UK-IERI Thematic Partnership Award (2014-2017) between SMVD University and University of Cambridge (Grant No. F.184-6/2015); (c) The Natural Environment Research Council Impact Acceleration Award, UK (NERC-IAA) Knowledge Exchange Awards 2014; (d) NERC International Opportunities Fund (NERC-IOF) 2015; (e) UGC Major Research Project (F.No. 43538/2014(SR)) awarded to SMVD University and IISER Kolkata (2015-2017), and (f) The Royal Society International Collaboration Awards 2018 (Grant Ref: ICA/R1/180234) between University of Cambridge and IISER Kolkata. Seismological data preprocessing and part of the analysis was performed using Seismic Analysis Code, version 101.6a (Goldstein et al., 2003) and the Computer Programs in Seismology v330 (Herrmann, 2013). All plots were made using the Generic Mapping Tools version 5.4.3 (Wessel et al., 2013). SM acknowledges IISER Kolkata Academic Research Fund (ARF). SM and SKW acknowledge Cambridge-Hamied visiting fellowship. SS acknowledges DST INSPIRE PhD fellowship and support from the above listed international grants to visit

the Bullard Labs, University of Cambridge, on multiple occasions and conduct a part of her PhD research.

References

- Acton, C., Priestley, K., Mitra, S., & Gaur, V. (2011). Crustal structure of the Darjeeling–Sikkim Himalaya and southern Tibet. *Geophys. J. Int.*, *184*, 829–852.
- Ader, T., Avouac, J.-P., L., Z. J., Lyon-Caen, H., Bollinger, L., Galetzka, J., ... Flouzat, M. (2012). Convergence rate across the nepal himalaya and interseismic coupling on the main himalayan thrust: Implications for seismic hazard. *J. Geophys. Res.*, *117*(B4), B04403.
- Ammon, C., Randall, G., & Zandt, G. (1990). On the nonuniqueness of receiver function inversions. *J. Geophys. Res.*, *95*, 15,303–15,318.
- Ammon, C. J. (1991). The isolation of receiver effects from teleseismic P waveforms. *Bulletin of the Seismological Society of America*, *81*(6), 2504–2510.
- Avouac, J.-P., Ayoub, F., Leprince, S., Konca, O., & Helemberger, D. (2006). The 2005, Mw 7.6 Kashmir earthquake: Sub-pixel correlation of ASTER images and seismic waveform analysis. *Earth Planet. Sc. Lett.*, *249*, 514–528.
- Bilham, R. (2019). Himalayan earthquakes: a review of historical seismicity and early 21st century slip potential. *Geol. Soc. Spec. Publ.*, *483*, SP483–16.
- Bilham, R., Gaur, V., & Molnar, P. (2001). Himalayan seismic hazard. *Science*, *293*, 1442–1444.
- Caldwell, W., Klemperer, S., J.F., L., Rai, S. S., & Ashish. (2013). Characterizing the Main Himalayan Thrust in the Garhwal Himalaya, India with receiver function CCP stacking. *Earth Planet. Sc. Lett.*, *367*, 15–27.
- Crotwell, H. P., Owens, T. J., Ritsema, J., et al. (1999). The taup toolkit: Flexible seismic travel-time and ray-path utilities. *Seismological Research Letters*, *70*, 154–160.
- Dueker, K. G., & Sheehan, A. F. (1997). Mantle discontinuity structure from mid-point stacks of converted P to S waves across the Yellowstone hotspot track. *J. Geophys. Res.*, *102*(B4), 8313–8327.
- Gavillot, Y., Meigs, A., Yule, D., Heermance, R., Rittenour, T., Madugo, C., & Malik, M. (2016). Shortening rate and Holocene surface rupture on the Riasi

- 667 fault system in the Kashmir Himalaya: active thrusting within the Northwest
668 Himalayan orogenic wedge. *Bulletin*, 128(7-8), 1070–1094.
- 669 Gilligan, A., & Priestley, K. (2018). Lateral variations in the crustal structure of the
670 indo-eurasian collision zone. *Geophysical Journal International*, 214(2), 975–
671 989.
- 672 Goldstein, P., Dodge, D., Firpo, M., & Minner, L. (2003). Sac2000: Signal process-
673 ing and analysis tools for seismologists and engineers. In W. Lee, H. Kanamori,
674 P. Jennings, & C. Kisslinger (Eds.), *The iaspei international handbook of earth-
675 quake and engineering seismology*. London: Academic Press.
- 676 Herrmann, R. B. (2013). Computer Programs in Seismology: An evolving tool for
677 instruction and research. *Seismol. Res. Lett.*, 84, 1081–1088.
- 678 Herrmann, R. B., & Ammon, C. J. (2004). *Computer Programs in Seismology: Sur-
679 face waves, Receiver Functions and Crustal Structure*. Saint Louis University,
680 St. Louis, MO.
- 681 Huang, X., Gurrola, H., & Parker, J. (2015). A comparative study of popular meth-
682 ods to compute receiver functions applied to synthetic data. *Seismological Re-
683 search Letters*.
- 684 Julià, J., Ammon, C., Herrmann, R., & Correig, A. (2000). Joint inversion of re-
685 ceiver function and surface wave dispersion observations. *Geophys. J. Int.*,
686 143, 99–112.
- 687 Kennett, B., & Engdahl, E. (1991). Traveltimes for global earthquake location and
688 phase identification. *Geophys. J. Int.*, 105(2), 429–465.
- 689 Khattri, K. (1987). Great earthquakes, seismicity gaps and potential for earthquake
690 disaster along the himalaya plate boundary. *Tectonophysics*, 138(1), 79–92.
- 691 Kumar, A., Singh, S. K., Mitra, S., Priestley, K., & Dayal, S. (2017). The 2015
692 april 25 Gorkha (Nepal) earthquake and its aftershocks: Implications for lat-
693 eral heterogeneity on the Main Himalayan Thrust. *Geophys. J. Int.*, 208(2),
694 992–1008.
- 695 Langston, C. A. (1977). Corvallis, Oregon, crustal and upper mantle receiver struc-
696 ture from teleseismic P and S waves. *Bulletin of the Seismological Society of
697 America*, 67(3), 713–724.
- 698 Ligorria, J., & Ammon, C. (1999). Iterative deconvolution and receiver-function esti-
699 mation. *Bull. Seismol. Soc. Am.*, 89, 1395–1400.

- 700 Mir, R. R., Parvez, I. A., Gaur, V. K., Chandra, R., & Romshoo, S. A. (2017).
 701 Crustal structure beneath the Kashmir Basin adjoining the western Himalayan
 702 syntaxis. *Bulletin of the Seismological Society of America*, 107(5), 2443–2458.
- 703 Mitra, S., Priestley, K., Gaur, V., & Rai, S. (2006). Shear-wave structure of the
 704 south Indian lithosphere from Rayleigh wave phase-velocity measurements.
 705 *Bull. Seismol. Soc. Am.*, 96(4A), 1551–1559.
- 706 Mitra, S., Priestley, K. F., Borah, K. J., & Gaur, V. K. (2018). Crustal struc-
 707 ture and evolution of the eastern himalayan plate boundary system, north-
 708 east india. *J. Geophys. Res. B Solid Earth Planets*, n/a–n/a. Retrieved
 709 from <http://dx.doi.org/10.1002/2017JB014714> (2017JB014714) doi:
 710 10.1002/2017JB014714
- 711 Nábělek, J., Hetényi, G., Vergne, J., Sapkota, S., Kafle, B., Jiang, M., . . . others
 712 (2009). Underplating in the himalaya-tibet collision zone revealed by the
 713 hi-climb experiment. *Science*, 325(5946), 1371–1374.
- 714 O’Kane, A., Copley, A., Mitra, S., & Wimpenny, S. (2022). The geometry of active
 715 shortening in the northwest Himalayas and the implications for seismic hazard.
 716 *Geophys. J. Int.*, 231(3), 2009–2033. doi: 10.1093/gji/ggac303
- 717 Owens, T. J., Zandt, G., & Taylor, S. R. (1984). Seismic evidence for an ancient rift
 718 beneath the Cumberland Plateau, Tennessee: A detailed analysis of broadband
 719 teleseismic P-waveforms. *J. Geophys. Res.*, 89, 7783–7795.
- 720 Paul, H., Priestley, K., Powali, D., Sharma, S., Mitra, S., & Wanchoo, S. (2018).
 721 Signatures of the existence of frontal and lateral ramp structures near the
 722 kishtwar window of the jammu and kashmir himalaya: evidence from micro-
 723 seismicity and source mechanisms. *Geochemistry, Geophysics, Geosystems*,
 724 19(9), 3097–3114.
- 725 Powali, D., Sharma, S., Mandal, R., & Mitra, S. (2020). A reappraisal of the 2005
 726 kashmir (mw 7.6) earthquake and its aftershocks: Seismotectonics of nw hi-
 727 malaya. *Tectonophysics*, 789, 228501.
- 728 Priestley, K., Ho, T., & Mitra, S. (2019). The crust structure of the himalaya: a syn-
 729 thesis. *Geol. Soc. Spec. Publ.*, 483(<https://doi.org/10.1144/SP483-2018-127>).
- 730 Priestley, K., Zandt, G., & Randal, G. (1988). Crustal sturcture in eastern Kazakh,
 731 U.S.S.R. from teleseismic receiver functions. *Geophy. Res. Lett.*, 15, 613–616.
- 732 Schiffman, C., Bali, B. S., Szeliga, W., & Bilham, R. (2013). Seismic slip deficit

- 733 in the Kashmir Himalaya from GPS observations. *Geophys. Res. Lett.*, *40*(21),
 734 5642–5645.
- 735 Schulte-Pelkum, V., Monsalve, G., Sheehan, A., Pandey, M. R., Sapkota, S., Bilham,
 736 R., & Wu, F. (2005). Imaging the Indian Subcontinent beneath the Himalaya.
 737 *Nature*, *435*, 1222–1225.
- 738 Sharma, S. (2020). *Crust and upper mantle studies of j&k himalaya* (Doctoral dis-
 739 sertation, Shri Mata Vaishno Devi University, Katra). doi: [http://hdl.handle](http://hdl.handle.net/10603/316323)
 740 [.net/10603/316323](http://hdl.handle.net/10603/316323)
- 741 Sharma, S., Mitra, S., Sharma, S., Priestley, K., Wanchoo, S. K., Powali, D., & Ali,
 742 L. (2020). A report on broadband seismological experiment in the Jammu
 743 and Kashmir Himalaya (JAKSNET). *Seismological Research Letters*, *91*(3),
 744 1915–1926.
- 745 Singer, J., Kissling, E., Diehl, T., & Hetényi, G. (2017). The underthrusting indian
 746 crust and its role in collision dynamics of the eastern himalaya in bhutan: In-
 747 sights from receiver function imaging. *J. Geophys. Res. B Solid Earth Planets*,
 748 *122*(2), 1152–1178.
- 749 Stevens, V., & Avouac, J. (2015). Interseismic coupling on the Main Himalayan
 750 Thrust. *Geophys. Res. Lett.*, *42*(14), 5828–5837.
- 751 Thakur, V., & Rawat, B. (1992). *Geological map of the Western Himalaya*
 752 (Vol. 101). Authority of the Surveyor General of India, Survey of India.
- 753 Wang, M., & Shen, Z.-K. (2020). Present-day crustal deformation of continen-
 754 tal china derived from gps and its tectonic implications. *Journal of Geophysical*
 755 *Research: Solid Earth*, *125*(2), e2019JB018774.
- 756 Wessel, P., Smith, W. H., Scharroo, R., Luis, J., & Wobbe, F. (2013). Generic map-
 757 ping tools: improved version released. *Eos, Transactions American Geophysical*
 758 *Union*, *94*(45), 409–410.
- 759 Yu, H., Webb, A. A. G., & He, D. (2015). Extrusion vs. duplexing models of hi-
 760 malayan mountain building 1: Discovery of the pabbar thrust confirms duplex-
 761 dominated growth of the northwestern indian himalaya since mid-miocene.
 762 *Tectonics*, *34*(2), 313–333.
- 763 Zhu, L. (2000). Crustal structure across the San Andreas fault, southern California
 764 from teleseismic converted waves. *Earth and Planetary Science Letters*, *179*(1),
 765 183–190.